Solar Energy Materials & Solar Cells 206 (2020) 110329

Contents lists available at ScienceDirect

Solar Energy Materials and Solar Cells

journal homepage: http://www.elsevier.com/locate/solmat

Application of polycrystalline silicon carbide thin films as the passivating contacts for silicon solar cells

Zhiyu Xu [a,b], Ke Tao [b,*], Shuai Jiang [b], Rui Jia [b,*], Wei Li [a,***], Ying Zhou [b], Zhi Jin [b], Xinyu Liu [b]

[a] School of Electrical and Electronic Engineering, Tianjin Key Laboratory of Film Electronic & Communication Devices, Tianjin University of Technology, Tianjin, 300384, China

[b] Institute of Microelectronics of Chinese Academy of Sciences, 3# Bei-Tu-Cheng West Road, Beijing, 100029, China

ARTICLE INFO

Index Terms:
Silicon carbide thin film
PECVD
Optical band gap
Passivation contact

ABSTRACT

In this paper, silicon rich polycrystalline silicon carbide (poly-SiCx) thin films were prepared for passivating contact of silicon solar cells. The effect of different carbon doping ratios R [methane flow (sccm)/silane flow (sccm)] and the annealing temperatures on the passivation quality was investigated. The lifetime test showed that, given a lower annealing temperature, the passivation quality of poly-SiCx thin films was very poor at R over 0.2, and it can be improved by elevating the annealing temperature. The effective lifetime of over 1.8 ms can be obtained with implied open-circuit voltages (iVoc) of 715 mV and saturated dark current (J_0) of 18 fA/cm^2. The microstructure and optical property of poly-SiCx films was studied by Raman spectra, X-ray photoelectron spectroscopy and UV-VIS spectrophotometer. The results showed that the incorporation of carbon lowered the crystalline fraction of poly-SiCx and a higher annealing temperature was needed to achieve high crystallinity. The optical band gap of poly-SiCx was widened with increase in R, and got up to 2.3eV when R was 0.4. A proof-of-concept top/rear TOPCon solar cells, featuring a N^+-poly-SiCx (R = 0.2) front contact, was fabricated to demonstrate the potential of this SiCx passivation contact. The decrease in the parasitic absorption of light at the front side resulted in higher photogenerated current. And the conversion efficiency of 20.17% was achieved.

1. Introduction

The conversion efficiency of crystalline silicon solar cells has been increasing continuously after the invention of solar cell and has been further improved by lowering the recombination of charge carriers at direct metal-semiconductor interfaces. The current industrial trend is to define partial rear contact, like PERC solar cells [1]. However, this reduced contacted area leads to the increase in series resistance and thus the decrease in fill factor (FF). Another strategy named "passivating contact" has been developed to decrease the recombination loss. The passivating contact combines a thin buffer layer for surface passivation and a highly doped contact layer for selectively collecting carriers. The best example for passivating contact integration is the heterojunction-based Si solar cells which firstly achieved an efficiency over 25% and created the current world-record efficiency for single-junction c-Si solar cells [2,3]. However, it is not compatible with industrial fire-through metallization schemes since the amorphous silicon can not withstand temperature above 250 °C. Another promising approach to obtain better temperature stability is the tunnel oxide passivated contact (TOPCon) solar cells which was first proposed by the fraunhofer institute of solar energy in Germany in 2013 [4]. This structure consists of an ultra-thin silicon oxide film and a highly doped polycrystalline silicon film thin layer [5]. TOPCon structure featuring favourable surface passivation effect and good thermal stability can achieve selective contact of carriers. Owing to its excellent passivation and junction properties, remarkable cell efficiency up to 25.7% has been reported, which is the world record for both sides-contacted silicon solar cell [6].

This paper addresses solar cells with TOPCon structure on both sides [7]. In-situ doped SiCx thin films were adopted as the passivating contact at the front side of cells [8,9]. SiCx material has several advantages: the wide optical band gap to reduce the parasitic absorption of light and improve the blue light response of the cell [10]; another one is the higher resilience to blistering than that of Si:H thin film during the

* Corresponding author.
** Corresponding author.
*** Corresponding author.
E-mail addresses: taoke@ime.ac.cn (K. Tao), imesolar@126.com (R. Jia), cliwei618@126.com (W. Li).

https://doi.org/10.1016/j.solmat.2019.110329
Received 27 August 2019; Received in revised form 29 November 2019; Accepted 29 November 2019
Available online 6 December 2019
0927-0248/

high-temperature annealing. Because the C–H is more stable than that of Si–H bond with respect to hydrogen effusion [11]. The motivation of this work is to demonstrate the promising properties of poly-SiCx thin film as a passivating contact in high-efficiency silicon solar cell. Compared with the previous works on this topic, different experimental results have been observed. For example, with the increase in the gas flow ratio R between CH_4 and SiH_4, the effective minority carrier lifetime of samples decreased drastically given the relatively low annealing temperature. Interestingly, at 900 °C, the carrier lifetime increased in the beginning and achieved its maximum at R = 0.3. Moreover, at 950 °C, the carrier lifetime increased gradually with the R in the whole range (0–0.4). The results suggested that the both the annealing temperature and the doping ratio of carbon played important role in the passivation quality of poly-SiC_x.

The passivation quality, the optical property and the microstructure of the SiCx thin film as a function of carbon content will be discussed. Finally, a proof-of-concept top/rear TOPCon solar cells will be developed.

1.1. Experiment

To characterize the passivation properties of the poly-SiCx/SiOx, samples with double-sided symmetrical structure were prepared for testing, as shown in Fig. 1. Phosphorus doped <100> oriented CZ silicon wafers with a thickness of 200 μm, a resistivity of 1–3 Ω cm were used as substrate. The wafers were firstly chemically cleaned by a RCA process, followed by a HF-dip to remove the surface oxide. Then the tunnel oxide layer was grown in 70 wt% HNO_3 acid at 110 °C for 10 min [12,13]. The thickness of the tunneling oxide layer measured by ellipsometer was about 1.4 nm. After that, we used three-chamber PECVD system with a ratio frequency of 13.56 MHz to deposit SiCx thin films. The deposition temperature was 200 °C and the pressure was 70Pa. The mixed gas of H2 and SiH4 serves as the gas sources. The doping ratio of carbon was defined as R = [methane flow (sccm)/silane flow (sccm)]. A subsequent high temperature annealing in N2 atmosphere was carried out to crystallize the SiCx thin films. The annealing temperature is in between 800 °C and 950 °C and the annealing time was 5 min. Forming Gas Annealing (5% H_2 diluted in N_2) at 450 °C was performed to further improve the contact passivation.

Film thickness was evaluated by spectroscopic ellipsometry (SE400, Sentech, Germany), and micro-structure was characterized by Raman spectra. The doping profiles were measured by electrochemical capacitance-voltage (ECV) profiling (CVP21, WEP, Germany). The implied open-circuit voltage (iVoc) and effective minority carrier lifetime (τ_{eff}) were obtained by quasi-steady-state photoconductance (QSSPC) method (WCT-120, Sinton Instruments, USA). XPS (ESCALAB 250Xi) was measured to analyze the composition change and specific chemical bond structure of each element in SiCx thin films. In order to investigate the optical property of poly-SiCx thin film, SiCx thin films were deposited on quartz glass, with the thickness of about 90 nm. The transmittance and reflectance spectra of quartz/SiOx/poly-SiCx/air system were measured by the UV-VIS spectrophotometer (Cary 7000) in the wavelength ranging from 200 nm to 800 nm.

TOPCon solar cells with 2 × 2 cm^2 area were fabricated employing the N^+-poly-SiCx on the textured front side and the P^+-poly-Si on the planar rear side, and the schematic of solar cell structure has been shown in Fig. 1(b). N-type CZ silicon wafers with a thickness of 200 μm, a resistivity of 1–3 Ω cm were firstly cleaned by standard RCA process. Secondly, the ultrathin chemical oxide layer was grown on the both side of silicon wafer. Thirdly, N-a-SiCx thin film and p-a-Si thin film were deposited by PECVD on the front side and the rear side, respectively. And then the N^+-poly-SiCx and P^+-poly-Si contacts were realized on the front and rear by a single coannealing step (850 °C, 5min) in N_2 atmosphere in a quartz tube furnace. After that a transparent conductive oxide ITO thin film with thickness of 80 nm were deposited on the front side by a RF magnetron sputtering system. Then, 1 μm-thick Al electrodes were prepared by e-beam evaporator on both side of substrate. Finally, the substrate was diced into several small solar cells, and the surface area of each cell was about 4 cm^2. The light J-V characteristics of solar cells were measured under AM1.5 solar simulator at 25 °C. The external quantum efficiency (EQE) was measured via 7-SCSpec solar cell spectral measurement system.

2. Results and discussions

2.1. Surface passivation property of SiOx/poly-SiCx

Fig. 2 shows the effective carrier lifetime (τ_{eff}) of poly-SiCx/SiOx passivated structure as a function of carbon doping ratio R and the annealing temperature. Here the thickness of SiCx thin film was about

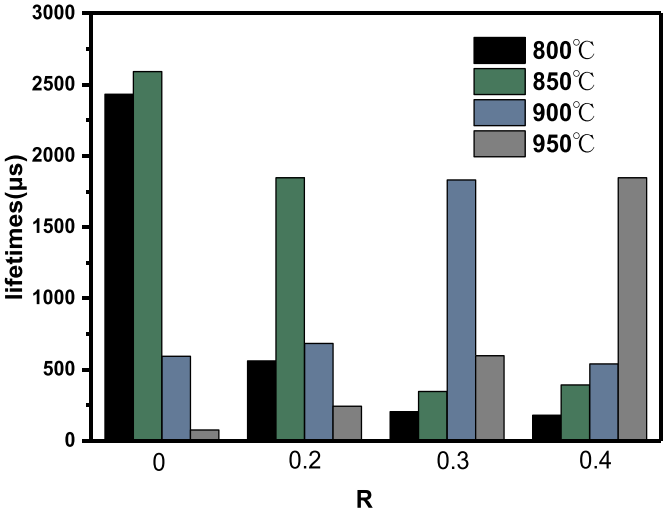

Fig. 2. The effective carrier lifetime of samples with different R values at annealing temperature of 800 °C, 850 °C, 900 °C and 950 °C for dwell time of 5min, the injection level is 5 × 10^{15}cm-3.

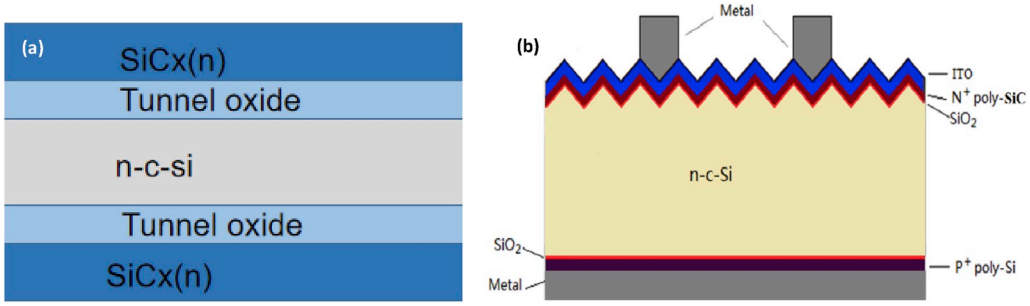

Fig. 1. Schematic diagram of passivation contact structure.

22 nm (measured before annealing). When the gas flow rate of methane was 0 sccm (R = 0), the τ_{eff} obtained its maximum of ~2.5 ms (@5 × 10^{15}/cm^3) at annealing temperature of 800–850 °C. Given higher annealing temperature, the τ_{eff} decreased drastically. With the increase in R, the τ_{eff} exhibited a slight decrease (to 1.8 ms@5 × 10^{15}/cm^3), and the optimum annealing temperature rose gradually: when R = 0.2, the optimum annealing temperature was 850 °C; when R = 0.3, the optimum annealing temperature was 900 °C; and when R = 0.4, the optimum annealing temperature was 950 °C. The resulted implied Voc (iVoc) for the three samples showed little difference (~715 mV) with similar saturated dark current (J_0) of about 18 fA/cm^2, suggesting that good passivation quality can be achieved at different conditions. This can be explained as follows: with the increase of methane flow, more carbon atoms were incorporated into the silicon thin film, leading to the increase of defect density in the film [14–16]. The increased defect density suppressed the crystallization and decreased the effective doping concentration of phosphorus, and this was further studied in the following subsections. As a result, the field passivation formed by the highly doped poly-SiCx films was weakened. Thus, given a larger R, it's necessary to raise the annealing temperature.

2.2. Electrochemical capacitance voltage measurements (ECV)

Fig. 3 (a) shows the doping profile of phosphorus atoms of poly-SiCx with different R [17]. Here, the annealing temperature was kept at 900 °C. It can be seen that the phosphorus diffused deeply into the silicon substrate when R was relatively small, e.g. R = 0, or 0.2. With increase R, the diffusion depth of phosphorus decreased gradually. That means the incorporation of carbon prevented the out-diffusion of phosphorus. In addition, the surface concentration of phosphorus tended to decrease when increasing R. Fig. 3(b) shows the doping profile of phosphorus atoms of poly-SiCx annealed under different temperatures (800 °C, 850 °C, 900 °C, 950 °C). Here R was kept at 0.2. It can be seen that the higher the annealing temperature, the deeper the phosphorus diffused into silicon substrate. From Fig. 3, it also can be seen that the doping ratio R has the opposite effect on the diffusion depth of phosphorus when comparing with the annealing temperature. The reason may be related to the small atomic radius of carbon. The incorporation of carbon atoms helps to enhance the atomic density of the silicon thin film, which inhibits the out-diffusion of phosphorus atoms. Thus, a larger R resulted in a more compact structure of silicon film and finally a shallower diffusion of phosphorus [18]. Further study will be conducted to confirm it. Besides, given a bigger R, the effective doping concentration of phosphorus turned to be decrease, which led to a weak field passivation. If the annealing temperature was further raised, the tunnel oxide may be destroyed, which can also lower the lifetime. From this point, further increase in R may result in a lower τ_{eff} [19].

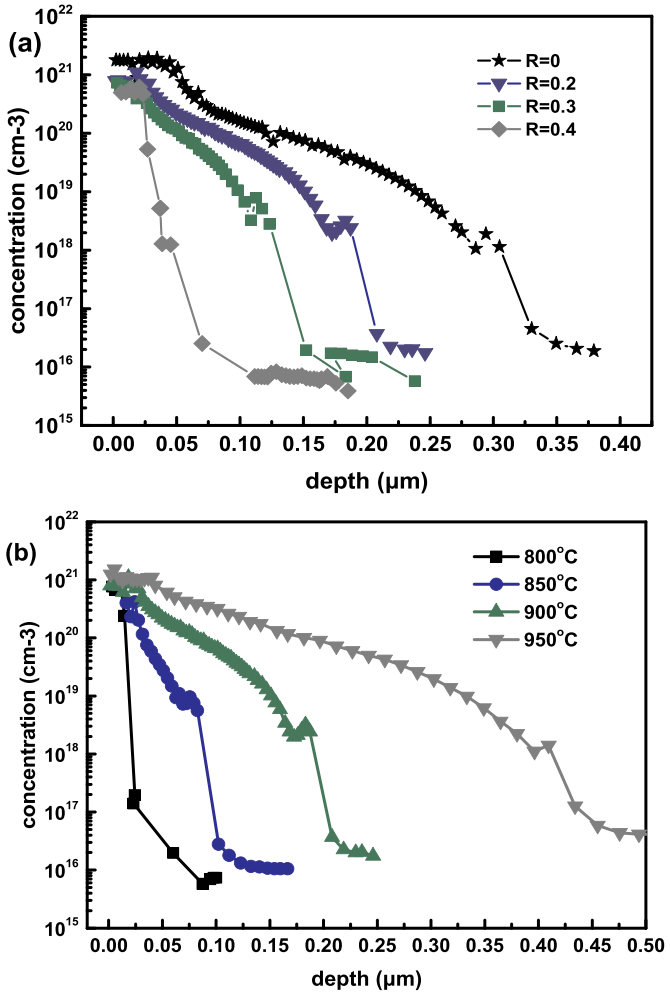

Fig. 3. (a) The doping profile of N^+-poly-SiCx samples at various R when annealing at 900 °C, and (b) the doping profile of N^+-poly-SiCx samples at different annealing temperature when R = 0.2.

2.3. Raman characterization

In order to investigate the microstructure of SiCx thin films, Raman spectra was measured. The SiCx thin films prepared with different R were deposited on quartz glass covered by a thin silicon oxide layer. Fig. 4 (a)~(c) display the Raman spectra of SiCx thin films prepared with different R. All the samples exhibited a strong peak near 520 cm^{-1}, indicating a big crystallinity of those SiCx thin films [20]. At the same time, with increasing the annealing temperature, the peak intensity turned big gradually for all the samples. This meant that a higher temperature can help to crystallize the SiCx thin film [21]. On the contrary, with increase in R, the peak intensity decreased, suggesting that the corporation of carbon was bad for the crystallization of SiCx thin film.

Using gaussian 3-peak fitting, the Raman spectra can be divided into 3 peaks, which located at 480 cm^{-1}, 510 cm^{-1} and 520 cm^{-1}, respectively. The peaks at 480 cm^{-1} and 520 cm^{-1} corresponded to the TO mode of amorphous silicon and crystalline silicon respectively. The peak at 510 cm^{-1} related to the mixed state of grain boundary. The crystalline fraction of the annealed SiCx thin films can be calculated by formula (1) [22]:

$$X_c = \frac{I_{520} + I_{510}}{I_{520} + I_{510} + I_{480}} \quad (1)$$

Where X_c is the crystallinity, I_{480}, I_{510} and I_{520} are the integral area of peaks at 480 cm^{-1}, 510 cm^{-1} and 520 cm^{-1} respectively. As summarized in Fig. 4(d), the maximum crystallinity of SiCx thin film was up to 74% when R = 0.2 and the annealing temperature was 950 °C. With increase in R (≥0.3), the crystallinity exhibited a large decrease (~10%).

2.4. Optical properties of SiCx thin films

The optical properties of SiCx thin films have been investigated by Cary 7000 uv–visible spectrophotometer. A group of SiCx thin films were deposited on quartz glass substrate with various R, and all the samples were annealed at 850 °C. The transmittance and reflectance spectra of samples were tested, and Tauc curve was used to calculate the optical band gap, using formula (2), as shown in Fig. 5(a). The optical band gap of SiCx thin film as a function of R was displayed in Fig. 5(b). As can be seen that the optical band gap increased gradually as the increase in R and reached a value of 2.3 eV when R was 0.4. The increase in optical band gap can be explained by considering the bond length of the Si–C which was smaller than that of Si-Si [23].

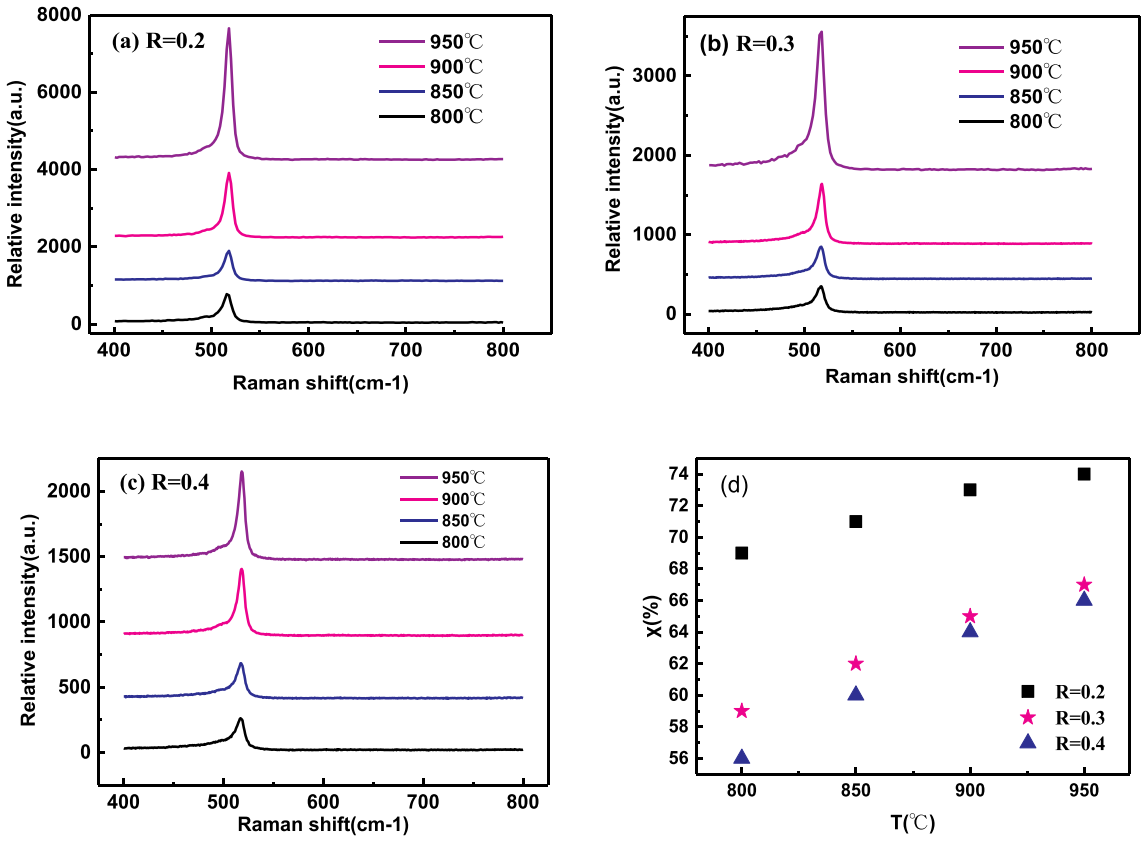

Fig. 4. Raman spectra of silicon carbide samples with (a) R = 0.2, (b) R = 0.3 and (c) R = 0.4 at 800 °C, 850 °C, 900 °C and 950 °C, and the crystalline fraction of the samples are summarized in (d).

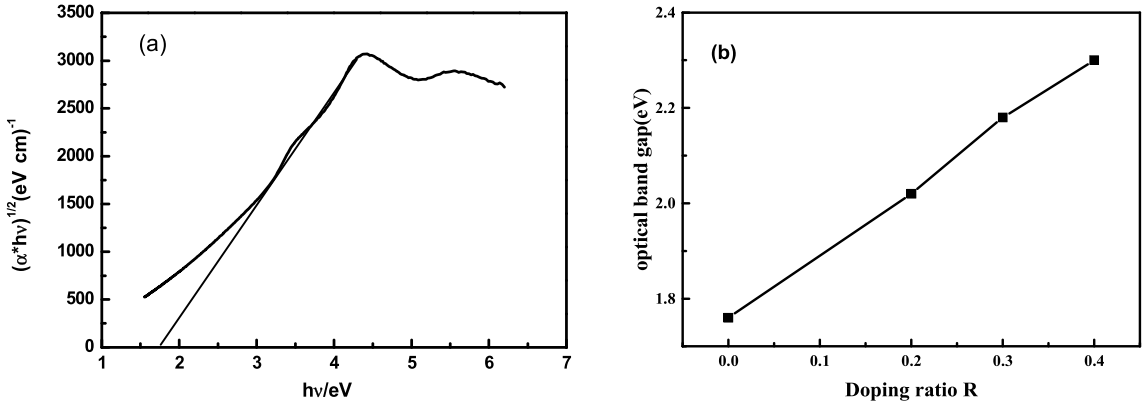

Fig. 5. (a) Tauc curve of samples when R = 0, and (b) The optical band gap of SiCx thin film as a function of R.

$$(\alpha h\nu)^{1/2} = B\left(h\nu - E_g\right) \quad (2)$$

Where: hν is photon energy, B is constant, α is the absorption coefficient and E_g is the optical band gap.

2.5. XPS analysis

In order to quantitatively analyze the chemical composition and bonding states of the deposited poly-SiCx thin films, XPS measurement was performed for the samples. From the full XPS survey spectra (not shown here), the Si2p, C1s and O1s peaks were observed at 101.5, 285 and 533eV, respectively [24–26]. It is well known that XPS only measures the chemical bonds on the surface of samples, so the oxygen contamination of surface can be attributed to the oxidation in the high temperature annealing process and the exposure to air before the XPS research [27]. Narrow scan Si2p spectra of poly-SiCx thin films prepared with R = 0.2 and 0.4 and annealed at 850 °C are collected and fitted, as shown in Fig. 6. With the Gaussian fit, Si2p spectra are decomposed into three main modes, corresponding to Si–Si peak (located at 99.7eV), Si–C peak (located at 100.3ev) and Si–O peak (located at 103ev). By comparison of Fig. 6(a) and (b), similar narrow scan spectra were observed for the two samples. However, the peak of Si–C mode in Fig. (b) was stronger than that in Fig. (a), indicating an increase in the carbon content.

2.6. F. top/rear TOPCon solar cells

A proof-of-concept top/rear TOPCon solar cells, featuring a N^+-poly-

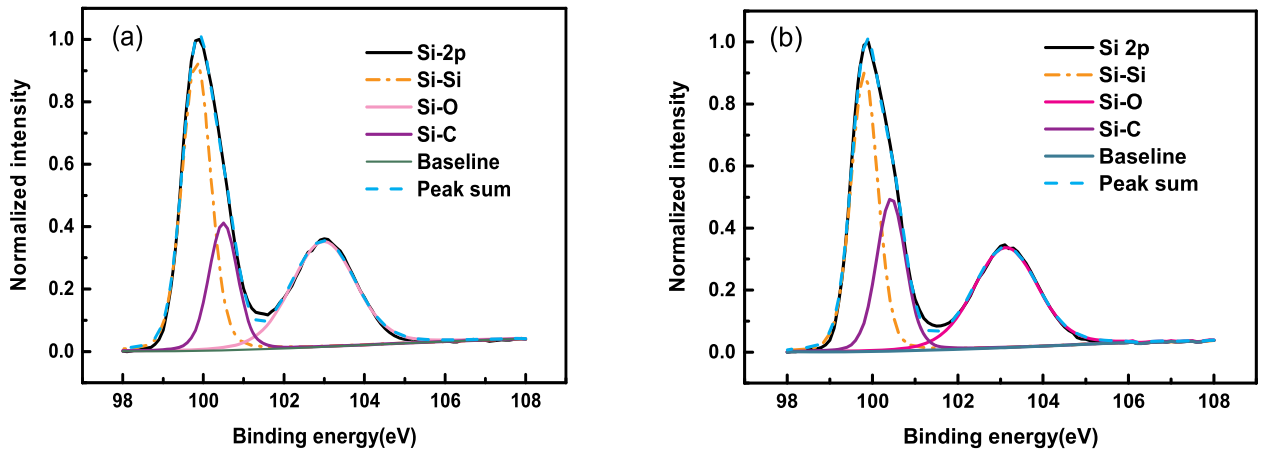

Fig. 6. Si2p narrow scan spectra of poly-SiCx films with (a) R = 0.2 and(b) R = 0.4.

SiCx (R = 0.2) front contact, have been fabricated to demonstrate the potential of this SiCx passivation contact. It should be noted that, during the fabrication of solar cell devices, a single coannealing step was adopted to crystallize both the n-a-SiCx thin film and p-a-Si thin film. Thus, the annealing temperature chosen must be suited for p-a-Si films. Our previous works found that the annealing temperature of p-a-Si films should be lower than 850 °C, so that a good passivation quality of p-type TOPCon can be obtained. Therefore, R of 0.2 was chosen to fabricate solar cells. Another group of TOPCon solar cells with N^+-poly-Si (R = 0) thin films as the front contacts have been prepared for comparison. Here, the thickness of both N^+-poly-SiCx and N^+-poly-Si thin films was about 15 nm. ITO thin films with thickness of 80 nm was deposited on phosphorus-doped N+ poly-Si(C) films at room temperature, and the sputtering power was 40W. Before metallization, all the solar cells were annealed at 500 °C for 60 min to recover the sputtering damage [28]. For the rear side of solar cells, p-type TOPCon was adopted. The passivation quality of p-type TOPCon was evaluated by a symmetric structure. The J_0 values were determined from the slope of the inverse Auger-corrected injection level dependent effective lifetime at high-injection conditions. The Jo and iVoc were 35.5fA/cm^2 and 694 mV, respectively. The output performance of the two groups of solar cells has been shown in Fig. 7(a). It can be seen that solar cells with poly-Si front contact exhibited a poor performance especially Jsc (36.25 mA/cm^2). On the contrary, a Jsc of 37.72 mA/cm^2 was obtained when poly-SiCx was used as the front contact, and the conversion efficiency was improved from 19.07% to 20.17%. This phenomenon can be understood by considering the parasitic absorption of poly-Si thin film at the front side of solar cells. The incorporation of carbon atoms widened the band gap of silicon thin film, as a result, the parasitic absorption loss of light was reduced and more photogenerated carrier can be produced. The external quantum efficiency curves (EQE) curves of solar cells were displayed in Fig. 7(b). It can be seen that an obvious improvement of EQE at the short wavelength range was obtained when poly-SiCx thin film was used as the front contact. This result corresponded well with the solar cell performance.

The experimental results above suggest that poly-SiCx thin films have wide optical band gap (up to 2.3 eV when R = 0.4), which is useful for solar cell to reduce the optical loss. Besides, under a certain condition, poly-SiCx thin films can provide high passivation quality comparable to that of poly-Si films. This characteristic is beneficial for solar cells to obtain the high open circuit voltage.

3. Conclusion

In this work, N^+-poly-SiCx thin films have been investigated for the passivation contact. The symmetric lifetime test showed that the incorporation of carbon degraded the passivation quality. Given a bigger doping ratio R of carbon, a higher annealing temperature was essential for achieving high carrier lifetime. The detailed structure analysis showed that the incorporated carbon resulted in a compact structure,

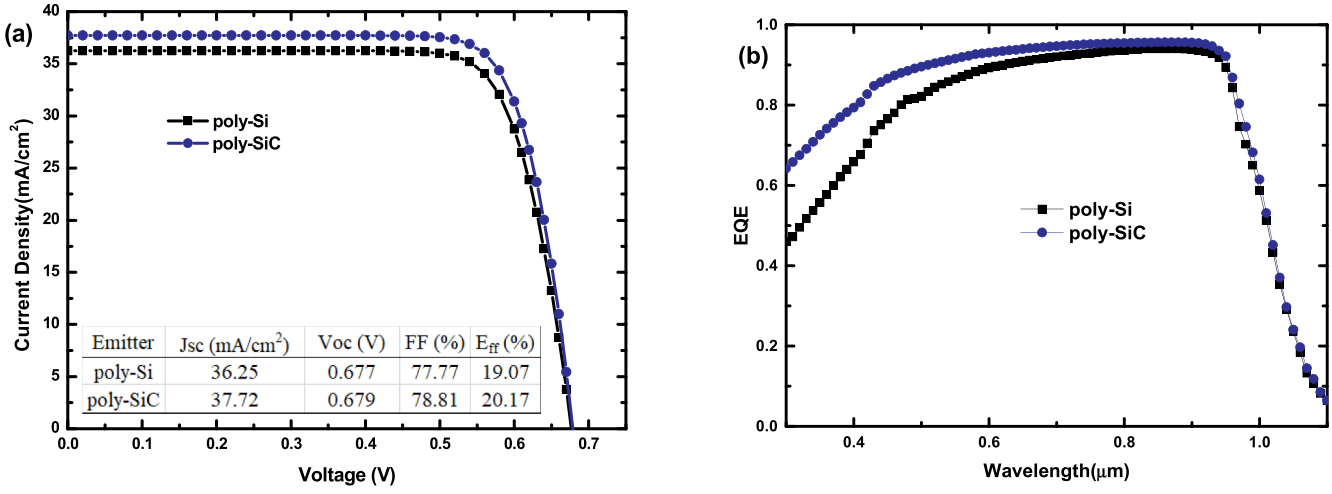

Fig. 7. (a) Light I–V curves for TOPCon solar cells with poly-Si and poly-SiCx front contacts. (b) External quantum efficiency (EQE) of solar cells with different window layers.

which prevented the phosphorus atoms in-diffusing into the silicon substrate during the annealing process, and the crystallinity of poly-SiCx decreased with increasing the carbon content. Besides, the elevated annealing temperature can help to improve the crystalline fraction. Optical measurement demonstrated that the optical band gap of poly-SiCx increased with R and got up to 2.3 eV when R = 0.4. Top/rear TOPCon solar cells, which featured the poly-SiCx front contact, exhibited an obvious improvement of EQE at the short wavelength range when compared to that with poly-Si front contact. The resulted Jsc was increased from 36.25 to 37.72 mA/cm^2 and an efficiency of 20.17% was yielded by the poly-SiCx cells. The obtained results confirmed that the presented poly-SiCx contact outperformed the conventional poly-Si contact when adopted at the front side of solar cells.

Author contribution statement

Zhiyu Xu: Investigation; Data curation; Writing - original draft; Writing - review & editing; Ke Tao: Conceptualization; Project administration; Data curation; Writing - review & editing; Shuai Jiang: Software; Rui Jia: Conceptualization; Resources; Funding acquisition; Methodology; Data curation; Wei Li: Methodology; Formal analysis; Visualization; Ying Zhou: Investigation; Zhi Jin: Supervision; Xinyu Liu: Supervision.

Declaration of competing interest

The authors declare that they have no known competing financial interests or personal relationships that could have appeared to influence the work reported in this paper.

Acknowledgements

This work was supported by the National Key Research and Development Program of China (2018YFB1500500,2018YFB1500200), National Natural Science Foundation of China (NSFC, Grant Nos. 51602340, 51702355, 61804108), Natural Science Foundation of Beijing Municipality (4192064) and JKW Project 31512060106.

Appendix A. Supplementary data

Supplementary data to this article can be found online at https://doi.org/10.1016/j.solmat.2019.110329.

References

[1] A. Wolf, D. Biro, J. Nekarda, et al., Comprehensive analytical model for locally contacted rear surface passivated solar cells, J. Appl. Phys. 108 (2010) 124510.
[2] D. Adachi, J.L. Hernandez, K. Yamamoto, et al., Impact of carrier recombination on fill factor for large area heterojunction crystalline silicon solar cell with 25.1% efficiency, Appl. Phys. Lett. 107 (2015) 233506.
[3] K. Yoshikawa, H. Kawasaki, W. Yoshida, et al., Silicon heterojunction solar cell with interdigitated back contacts for a photoconversion efficiency over 26%, Nat. Energy 2 (2017) 17032.
[4] F. Feldmann, et al., Passivated rear contacts for high-efficiency n-type Si solar cells providing high interface passivation quality and excellent transport characteristics, Sol. Energy Mater. Sol. Cells 120 (Part A) (2014) 270–274.
[5] J. Stuckelberger, et al., Passivating electron contact based on highly crystalline nanostructured silicon oxide layers for silicon solar cells, Sol. Energy Mater. Sol. Cells 158 (2016) 2–10.
[6] A. Richter, et al., N-type Si solar cells with passivating electron contact: identifying sources for efficiency limitations by wafer thickness and resistivity variation, Sol. Energy Mater. Sol. Cells 173 (2017) 96–105.
[7] F. Feldmann, et al., Efficient carrier-selective p- and n- contacts for Si solar cells, Energy Mater. Sol. Cells 131 (2014) 100–104.
[8] A. Ingenito, G. Nogay, J. Stuckelberger, et al., Phosphorous-doped silicon carbide as front-side full-area passivating contact for double-side contacted c-Si solar cells, IEEE J. Photovolt. 9 (2019) 346–354.
[9] G. Nogaya, J. Stuckelbergera, P. Wyssa, et al., Interplay of annealing temperature and doping in hole selective rear contacts based on silicon-rich silicon-carbide thin films, Sol. Energy Mater. Sol. Cells 173 (2017) 18–24.
[10] L. Wang, J. Xu, T.F. Ma, et al., The influence of the growth conditions on the structural and optical properties of hydrogenated amorphous silicon carbide thin films, J. Alloy. Comp. 290 (1999) 273.
[11] W. Beyer, H. Wagner, F. Finger, Hydrogen evolution from a-Si: C:H and a-Si: Ge:H alloys, J. Non-Cryst. Solids 77 (1985) 857–860.
[12] H.K. Asuha, O. Maida, M. Takahashi, H. Iwasa, Nitric acid oxidation of Si to form ultrathin silicon dioxide layers with a low leakage current density, J. Appl. Phys. 94 (2003) 7328–7335.
[13] T. Kobayashi, O. Maida, M. Inoue, M. Takahashi, Y. Todokoro, H. Kobayashi, Ultrathin silicon dioxide layers with a low leakage current density formed by chemical oxidation of Si, Appl. Phys. Lett. 81 (2002) 3410–3412.
[14] T. Stapinski, G. Ambrosone, U. Coscia, et al., Defect characterization of a-SiC : H and a-SiN : H alloys produced by ultrahigh vacuum plasma enhanced chemical vapor deposition in different plasma conditions, Physica B 254 (1998) 99.
[15] Y. Zhang, P. Du, R. Zhang, et al., Structure and properties of hydrogenated amorphous silicon carbide thin films deposited by PECVD, J. Non-Cryst. Solids 354 (2008) 1435.
[16] I. Gunes, K. Sel, Effects of carbon content and plasma power on room temperature photoluminescence characteristics of hydrogenated amorphous silicon carbide thin films deposited by PECVD, Thin Solid Films 636 (2017) 85–92.
[17] E. Peiner, A. Schlachetzki, D. Krüger, Doping profile analysis in Si by electrochemical capacitance-voltage measurements, J. Electrochem. Soc. 142 (1995) 576–580.
[18] L. Jiang, X. Tan, T. Xiao, P. Xiang, The influence of methane flow rate on microstructure and surface morphology of a-SiC:H thin films prepared by plasma enhanced chemical vapor deposition technique, Thin Solid Films 622 (2017) 71–77.
[19] F. Feldmannetal, M. Simon, M. Bivour, et al., Efficient carrier-selective p- and n-contacts for Si solar cells, Sol. Energy Mater. Sol. Cells 131 (2014) 100–104.
[20] Z. Iqbal, S. Veprek, Raman scattering from hydrogenated microcrystalline and amorphous silicon, J. Phys. C Solid State Phys. 15 (1982) 377.
[21] H. Touir, et al., Bimodal crystal size distribution in annealed rf magnetron silicon films: a memory effect of the local order inhomogeneities in the initial amorphous state, J. Non-Cryst. Solids 227 (1998) 906–910.
[22] E. Bustarret, M.A. Hachicha, M. Brunel, Experimental determination of the nanocrystalline volume fraction in silicon thin films from Raman spectroscopy, Appl. Phys. Lett. 52 (1988) 1675.
[23] J. Bullot, M. Schmidt, Physics of amorphous silicon–carbon alloys, Phys. Status Solidi B 143 (1987) 345–418.
[24] Y. Zhang, Y. Hu, H. Zeng, et al., Silicon carbide recovered from photovoltaic industry waste as photocatalysts for hydrogen production, J. Hazard Mater. 329 (2017) 22.
[25] K. Yamamoto, Y. Koga, S. Fujiwara, XPS studies of amorphous SiCN thin films prepared by nitrogen ion-assisted pulsed-laser deposition of SiC target, Diam. Relat. Mater. 10 (2001) 1921.
[26] M. Li, L. Jiang, Y. Sun, et al., Silicon content influence on structure and photoluminescence properties of carbon rich hydrogenated amorphous silicon carbide thin films, J. Alloy. Comp. 753 (2018) 320–328.
[27] O.D. Coskun, T. Zerrin, Optical, structural and bonding properties of diamond-like amorphous carbon films deposited by DC magnetron sputtering, Diam. Relat. Mater. 56 (2015) 29–35.
[28] Ke Tao, Shuai Jiang, Rui Jia, et al., The impact of indium tin oxide deposition and post annealing on the passivation property of TOPCon solar cells, Sol. Energy 176 (2018) 241–247.